Research paper

Transformation of limonene into *p*-cymene over acid activated natural mordenite utilizing atmospheric oxygen as a green oxidant: A novel mechanism

Dimitra Makarouni[a,b], Sotiris Lycourghiotis[c], Eleana Kordouli[b], Kyriakos Bourikas[c], Christos Kordulis[b,d], Vassilis Dourtoglou[a,e,*]

[a] *VIORYL, Chemical and Agricultural industry, Scientific Research S.A., 28th km. Athens-Lamia national road, GR-19014, Afidnes, Greece*
[b] *Department of Chemistry, University of Patras, GR-26504, Patras, Greece*
[c] *School of Science and Technology, Hellenic Open University, Tsamadou 13-15, GR-26222, Patras, Greece*
[d] *Foundation of Research and Technology-Institute of Chemical Engineering Science (FORTH/ICE-HT) Stadiou Str. Platani, P.O. Box 1414, GR-26500, Patras, Greece*
[e] *Technological Educational Institute of Athens, Department of Oenology and Beverage Technology, 122 43, Athens, Greece*

A B S T R A C T

Natural mordenite originated from volcanic soils in Greek islands was treated with sulfuric acid aqueous solutions of different concentrations and solid mass/solution volumes. The samples were characterized using various techniques (N_2-physisorption, XRD, ATR-FTIR, SEM-EDS, TEM, Microelectrophoresis, Equilibrium pH) and tested in the transformation of limonene into *p*-cymene in the presence of atmospheric air at various temperatures and reaction times. The acid treatment is causing the removal of sodium oxide located inside the framework micropores and the small inter-fiber mesopores. This, in turn, increases drastically the BET specific surface area and unmasks negatively charged surface sites which are transformed into acid sites by adsorbing H^+/H_2O^+ ions. The relatively low extent removal of Al^{3+} ions does not disturb the framework of natural mordenite nor its fibrous morphology. The development of micropores and small mesopores surface area and surface acid sites are transforming the catalytically inactive natural mordenite into very active catalysts. The increase in the conversion and the yield of *p*-cymene follows the increase in the BET specific surface area. A novel mechanism was experimentally established involving a catalytic step followed by a non catalytic one. The first step involves adsorption of limonene on acid sites via the exocyclic double bond to form the more stable tertiary carbenium ion from which terpinolenes, terpinenes and "polymeric species" are formed. The "transition state shape selectivity" manifested by the catalysts studied does not allow the formation of intermediate disproportionation products. In the second step, catalyst-free aromatization and "polymerization" of terpinolenes and terpinenes were found to occur. The aromatization was proposed to proceed by abstraction of an allylic hydrogen resulting to free radical (R·) followed by combination with O_2 and radical chain propagation to yield allylic peroxides ([ROO·]) which by elimination of (HOO·) lead to the production of *p*-cymene. Moreover, high molecular weight compounds may be formed as radicals are combined to alkyl and peroxyl dimmers that may be polymerized. The experimental parameters concerning the acid treatment and reaction conditions were optimized for maximizing the amount of the produced *p*-cymene keeping as low as possible the amount of the produced polymeric species.

1. Introduction

The utilization of minerals as "natural" catalysts or catalytic carriers and of renewable raw materials for producing biofuels and useful products through green processes is very important for sustainable development in the frame of cyclic economy. In the present work activated natural mordenites are used for transforming limonene into *p*-cymene through a process involving catalytic and non-catalytic steps utilizing atmospheric oxygen as a green oxidant.

p-Cymene, one of the terpenes, is widely used as intermediate in the synthesis of fine chemicals for flavorings, fragrances, perfumes, fungicides, pesticides and non-nitrated musks [1–4]. In particular, *p*-cymene is also used for improving the odor of soaps and other industrial products and as solvent of dyes and varnishes as well [5]. Moreover, it is used as the starting material for the synthesis of *p*-cresol [6]. The traditionally used Friedel–Crafts alkylation of benzene and toluene [5] for

the synthesis of *p*-cymene involves the use of toxic substances. In addition, the use of homogenous acid catalysts creates serious problems concerning safety, corrosion and treatment of the disposed catalyst. The selective transformation of limonene into *p*-cymene is a promising green route [7–10]. This is because limonene is a cheap by-product of citrus (50,000 tons per year) and paper industry. Weaknesses related to the homogeneously catalyzed transformation of limonene into *p*-cymene (rather low yields of *p*-cymene, separation problems) turned the interest to heterogeneous catalysts. The transformation of limonene into *p*-cymene demands a solid catalyst with dual functionality: acid sites for isomerization – disproportionation and metallic sites for dehydrogenation steps involved in the whole process [11]. Thus, over high surface area solids provided only acid sites (silica, alumina, silica–alumina mixed oxides, zeolites, natural clays and active carbon) are obtained rather low yields in *p*-cymene. The deposition of metals on the surface of the aforementioned solids [Pd, Ag, Pt, Ni, Fe and Mn], developing dehydrogenation activity, is resulting to more active catalysts [12–15].

The mechanism for the catalytic transformation of limonene into *p*-cymene is widely reported [11,16–19]. A schematic representation is illustrated in Fig. 1. In the most of cases the reaction starts with the isomerization of limonene to other terpenes through migration of the exocyclic double bond into the ring (2). This is followed by ring dehydrogenation (5). Disproportionation of limonene (1) and the aforementioned intermediate terpenes (3) to 3-menthene, *p*-menth-1-ene, *p*-menthane and *p*-cymene followed by their dehydrogenation to *p*-cymene (4) is also frequently reported. Furthermore, in the most of cases large amounts high-molecular weight compounds, "polymers", are produced by polymerization [18,19]. Isomerization, disproportionation and polymerization proceed on acid sites through carbenium ion mechanisms. As the dehydrogenation step on metallic sites is endothermic the reaction should take place at relatively high

temperatures for obtaining acceptable yields in *p*-cymene.

For years it was considered that this mechanism described the transformation of limonene into *p*-cymene not only under inert atmosphere but also in open reactors in which the reaction mixture is in contact to the atmospheric oxygen [e.g. 17–19]. However, several years ago it has been reported that the limonene is auto oxidized slowly under air atmosphere forming mainly hydro peroxide [20]. On the other hand, air exposed α-terpinene is auto oxidized faster resulting to allylic epoxides and *p*-cymene as the major oxidation products and also hydrogen peroxide [21]. Finally, it has been reported that γ-terpinene can be effectively transformed into *p*-cymene in oxygen [22]. In particular, the peroxidation reaction of γ-terpinene results in *p*-cymene and a hydroperoxyl radical, which can be converted to hydrogen peroxide during the propagation step of the radical chain reaction. Under suitable temperature and oxygen pressure conditions very high yields in *p*-cymene were obtained whereas small amounts of polymeric compounds were formed through radical polymerization [22]. It should be stressed that in all cases the aforementioned transformations are taking place without catalysts.

In view of the above the critical question is whether the widely accepted reaction mechanism (Fig. 1) can be used for a full description of the limonene to *p*-cymene transformation taking place in the presence of air. What is the role of atmospheric oxygen in this case? Can it be used for achieving dehydrogenation of terpenes at relatively low temperatures instead of dehydrogenation on metallic sites working at higher temperatures? In order to investigate this alternative route we decided to study this transformation by combining acid, non-metallic, catalysts and atmospheric oxygen. Taking into account the prospect of using natural minerals as "physical" catalysts the choice of natural mordenite seems to be quite promising.

Mordenite is one of the most siliceous natural zeolites and the idealized chemical composition is $(Ca, Na_2, K_2)Al_2Si_{10}O_{24} \cdot 7H_2O$. A top
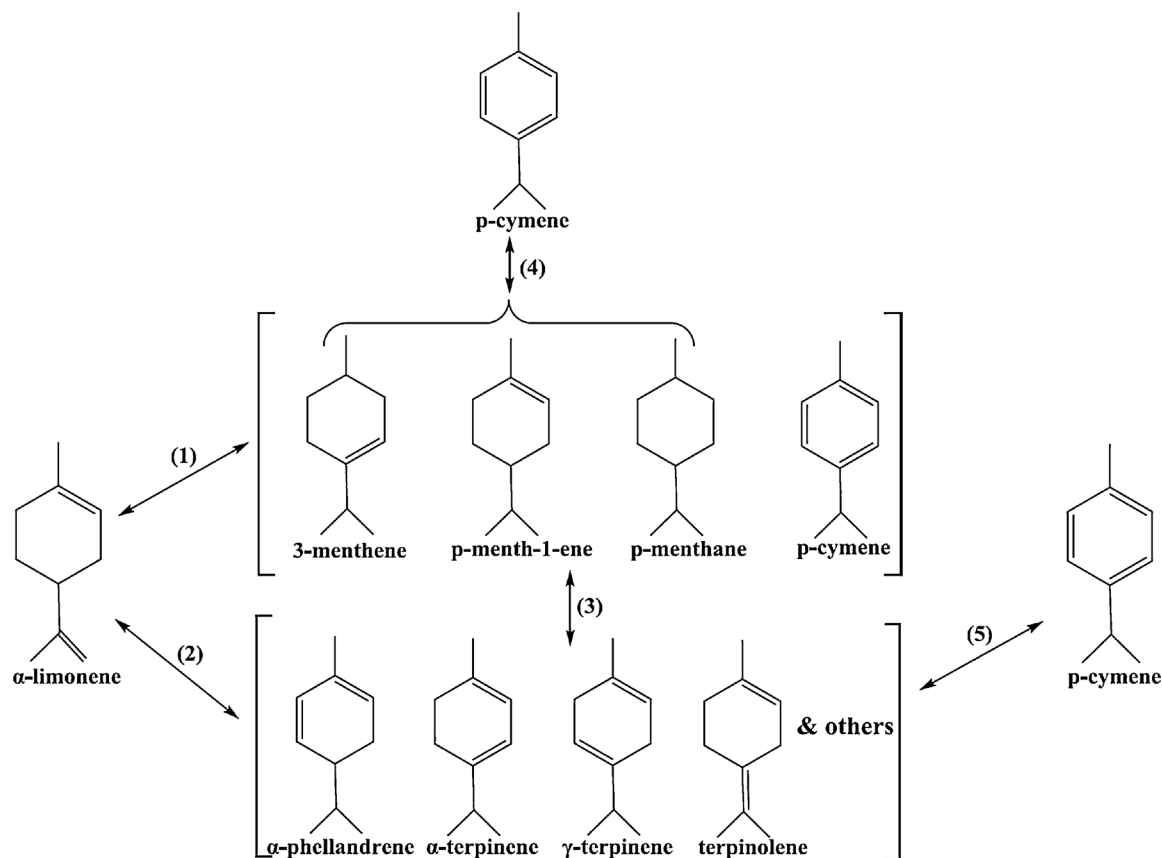

Fig. 1. Reaction network concerning the catalytic transformation of limonene into *p*-cymene [11].
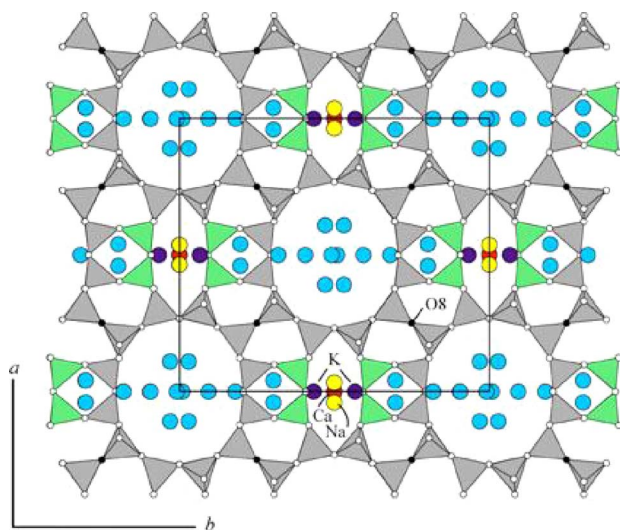
Fig. 2. Top view of the mordenite structure. It is composed of bound silicate (grey) and aluminate tetrahedrons (green). Larger channels, developed along axis c, are surrounded by 12 tetrahedrons (12MRc). Their aperture is about 0.67 nm × 0.7 nm [23,24]. The just smaller channels surrounded by eight tetrahedrons (8MRc) are about 0.34 nm × 0.48 nm [23,24]. These are grown along axis b. Thus the 12-membered ring main channels intersect with the 8-membered ring channels (side pockets). With blue, red, yellow, and purple circles, we represent, respectively, water molecules and the phases of calcium, sodium and potassium located inside the channels. (IZA commission on Natural zeolites). (For interpretation of the references to colour in this figure legend, the reader is referred to the web version of this article.)

view of its structure is shown in Fig. 2. Synthetic mordenite is one of the most important types of zeolite catalysts as it is industrially used in alkylation, hydroisomerization of light alkanes and dewaxing processes [25–27]. Therefore, the research concerns mainly synthetic mordenite. In this material the negative charge is compensated by H_2O^+ ions located inside the pore channels and in some cases by catalytically active ions introduced in the pores by ion exchange. The most important properties of synthetic mordenite are its relatively high acidity and the presence of uniform micropores which induce morphoselectivity. On the other hand, the small size of micropores imposes a low rate of intracrystalline diffusion of reactants and products and high probability of pore clogging. These problems could be addressed by treating mordenite with acids resulting to dealumination which causes the development of mesoporous structure and the decrease of the too high acidity [28–33]. Recent studies have shown that the acid treatment which bring about structural changes may improve the catalytic activity for several reactions such as the benzylation of benzene with benzyl alcohol to biphenyl methane [28], the oxidation of benzyl alcohol to benzaldehyde [29,30], the alkylation of cumene [31], the *n*-hexane isomerization [32] and the alkylation of benzene with 1-dodecene [33]. In these cases synthetic mordenite has been used. Studies concerning acid treatment of natural mordenite are very scarce [34].

In the present wok natural mordenite, which is originated from volcanic soils in Greek islands, is activated by treatment with sulfuric acid aqueous solutions of different volumes and concentrations. By the activation we are seeking the emptying of the natural mordenite micropores by removal of the solid phases located inside them in order to develop high surface area and surface acid sites without disturbing seriously the unique framework of the mineral. The resulting catalysts were characterized using various techniques and evaluated at various temperatures and reaction times in the presence of atmospheric air in order to optimize these parameters with respect to the yield of *p*-cymene. Catalytic experiments taking place in the presence of atmospheric oxygen or in inert atmosphere and non- catalytic experiments taking place in the presence of atmospheric oxygen were jointly elaborated to investigate the reaction mechanism.

2. Experimental

2.1. Preparation of the catalysts

2.1.1. Materials

The catalysts were prepared using natural mordenite not subjected previously to any kind of treatment. This is provided from the Greek company TECHNOTOPIA Ltd and originated from volcanic soils of Greek islands in the Aegean Sea. The extraction of the minerals was performed by the Greek company Bentomine Kimolian Enterprizes S.A. Liquid limonene (purity 95%) used for the catalytic tests was supplied by VIORYL S.A. It was extracted from natural orange oil and purified by distillation. Sulfuric acid and the tetraethylene glycol dimethyl ether were purchased from Fisher Scientific and BASF, respectively.

2.1.2. Acid activation of natural mordenite

Natural mordenite was stirred with distilled water for 2 h in a solid to volume ratio S(g)/L(ml) = 1/3. The undesirable materials (sand and residues) were removed by filtering (Sigma-Aldrich fine test sieve, SS frame, pore size 75 μm). The slurry was dried for 2 h at 90 °C. Finally, it was grinded to become fine-grained.

Sulfuric acid was used as the activating agent. The concentration of acid solutions and the ratio of mass of solid to solution volume were varied to see their effect on the textural, structural and catalytic properties. In a typical procedure the purified, fine-grained, mordenite and the acid solution were taken in a round-bottomed flask and the treatment was carried out at 70 °C for 4 h, followed by allowing it for cooling at room temperature. The solution was vacuum filtered (Büchner funnel sintered disc with porosity 2: 40–90 μm) and then the solid was double washed with distilled water in order to remove any acid left within mordenite pores. The wet cake obtained was then dried by heating at 100 °Covernight. Finally, it was grinded to become fine-grained. The acid activated mordenite catalysts prepared are involved in Table 1.

2.2. Physicochemical characterization

2.2.1. Nitrogen adsorption − desorption isotherms

0.1 g of the sample was used for determining the BET specific surface area as well the BJH specific surface area, specific pore volume and pore volume distributions of mesopores and small macropores. The determination was based on the nitrogen adsorption–desorption isotherms recorded using a Micromeritics apparatus (Tristar 3000 porosimeter) and the corresponding soft-ware.

2.2.2. X-ray diffraction

X-ray diffraction patterns were used for investigating the crystal structure of the samples. These were recorded in a BruckerD8 Advance diffractometer equipped with nickel-filtered CuKα (1.5418 Å) radiation source. The step size and the time per step were respectively fixed at 0.02° and 0.5s in the range of 0° ≤ 2θ ≤ 40°.

2.2.3. ATR-FTIR measurements

Attenuated Total Reflection-Fourier Transform Infrared (ATR-FTIR) spectra of all the samples were recorded on a FTIR Perkin-Elmer

Table 1
Parameters of the acid activation procedure and the symbols of the samples prepared.

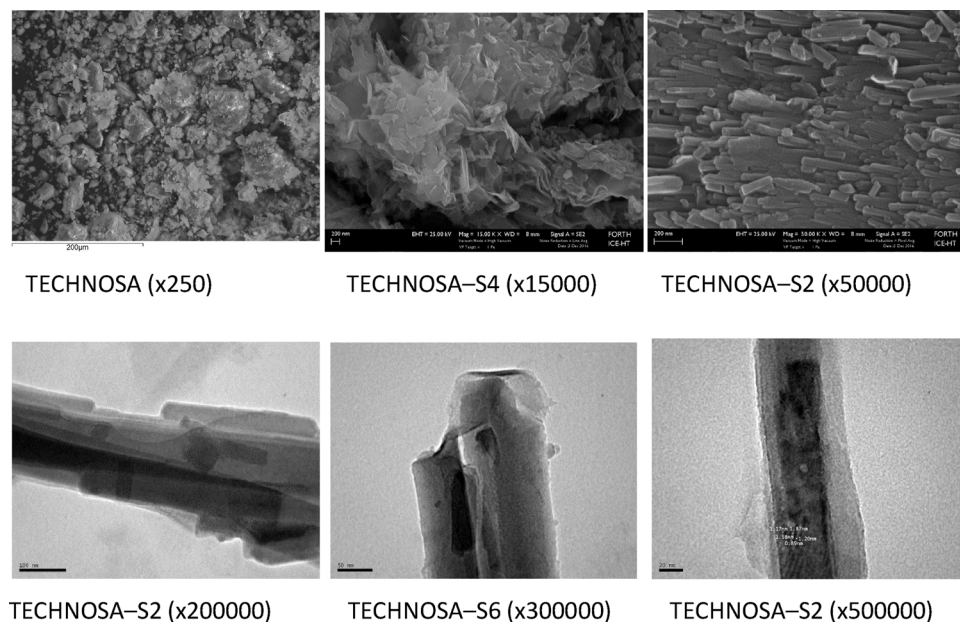| Sample code	Concentration of Sulfuric acid solution	Mass of solid to solution volume (g/mL)
TECHNOSA	–	–
TECHNOSA–S2*	2M	1:5
TECHNOSA–S2	2M	1:20
TECHNOSA–S4	4M	1:20
TECHNOSA–S6	6M	1:20

Fig. 3. Representative SEM (upper) and TEM (down) images of the samples studied at three different magnifications.

TECHNOSA (x250) TECHNOSA–S4 (x15000) TECHNOSA–S2 (x50000)

TECHNOSA–S2 (x200000) TECHNOSA–S6 (x300000) TECHNOSA–S2 (x500000)

Spectrum 100 spectrophotometer, using a multi-reflection horizontal ZnSe ATR accessory (Specac's Gateway ATR Accessory Kit). Spectra were recorded at $4 \, cm^{-1}$ nominal resolution in the range $800–4000 \, cm^{-1}$.

2.2.4. Scanning electron microscopy measurements

The determination of the elemental mapping was performed using a Scanning Electron Microscope (SEMJEOLJSM6300) equipped with an Energy Dispersive Spectrometer (EDS). The chemical composition of the samples was determined using natural and synthetic standards and 20 kV accelerating voltage with 10 nA beam current. Microanalysis was performed on gold coated samples. The sample powders were mounted directly on the sample holder.

2.2.5. Transmission electron microscopy measurements

A JEOL JEM-2100 system, operated at 200 kV (resolution: point 0.23 nm, lattice 0.14 nm), was used for conducting electron microscopy analysis of the samples.TEM images were recorded by means of an Erlangshen CCD Camera (Gatan, Model 782 ES500W). The specimens were prepared by dispersion in water and spread onto a carbon-coated copper grid (200 meshes).

2.2.6. Determination of the equilibrium pH of sample/water suspensions

The equilibrium pH of sample/water suspensions was used for estimating the acidity of the natural mordenite and the samples prepared. To determine this parameter we adopted the following procedure: 0.5 g of the solid sample was dispersed in 6.5 ml of distilled water. Stirring was followed to homogenize the suspension. The suspension was then allowed to stand in order to separate the liquid from the solid. After 10 min pH was measured with a pH-meter (Radiometer Copenhagen ABU901 Autoburet) equipped with a combination pH electrode. The electrode was calibrated with four Merck Titrisol NBS-standard buffer solutions between pH 3 and 11. The measurement in each sample was repeated after half an hour. No significant changes were observed between the two measurements.

2.2.7. Micro-electrophoresis measurements

Microelectrophoretic measurements were performed at 25 °C using a Zetasizer 5000 (Malvern Instruments Ltd). Very dilute sample/electrolyte suspensions (10 mg/100 mL) were prepared with constant ionic strength, 0.01 M $NaNO_3$. The pH of the suspensions was adjusted by small additions of a 1 M HNO_3 solution.

2.3. Determination of catalytic activity

Catalytic tests were performed in the presence of atmospheric oxygen in order to evaluate the catalytic performance concerning the transformation of limonene into p-cymene. Moreover, catalytic experiments taking place under inert atmosphere (N_2) and non-catalytic experiments taking place in the presence of atmospheric oxygen were jointly elaborated to investigate the reaction mechanism and evaluate the catalytic performance with respect to isomerization of limonene. 15 g of liquid limonene (purity 95%, peroxide value < 3), 15 g of tetraethylene glycol dimethyl ether (Peroxide value < 1) and 1 g of catalyst were placed in a three-necked round-bottom reaction flask equipped with a reflux condenser, thermometer and a Dean-Stark apparatus. In the experiments taking place under air atmosphere in the presence of catalyst the system was open allowing the contact of atmospheric oxygen with the reaction mixture. A connection to nitrogen supply was used for the experiments taking place in inert atmosphere in the presence of catalyst. Air was bubbled to the bottom of the flask in the experiment taking place without catalyst. The reaction flask was stirred vigorously and it was conventionally heated in an oil bath where temperature was adjusted. Different time periods and temperatures were tested. The resulting mixture was finally cooled to room temperature. By the end of the reaction the products were analyzed in a Gas chromatograph AGILENT Technologies 6890N with FID detector, using a Varian capillary column CP Sil 5 CB 25 m × 0.25 mm × 0.25 μm and He as the carrier gas, and by Gas chromatography-mass spectrometry, Shimadzu GCMA-QP2010 Ultra with column 20 m × 0.18 mm - × 0.18 μm and He as the carrier gas. Following the aforementioned procedure we have determined the percentage limonene conversion and the percentage product distribution.

3. Results and discussion

3.1. Morphology and chemical composition

Fig. 3 illustrates three representative SEM and TEM images taken at different magnifications (see more images in Fig. S1 and S2). It is seen that at very low magnifications the samples seem to have a rather granular morphology. A fibrous morphology emerges at higher magnifications indicating that the samples studied are ultimately consisted by very small fibers (width: tens nanometers) that are agglomerated to become larger ones. The initial fibers are separated by very small pores
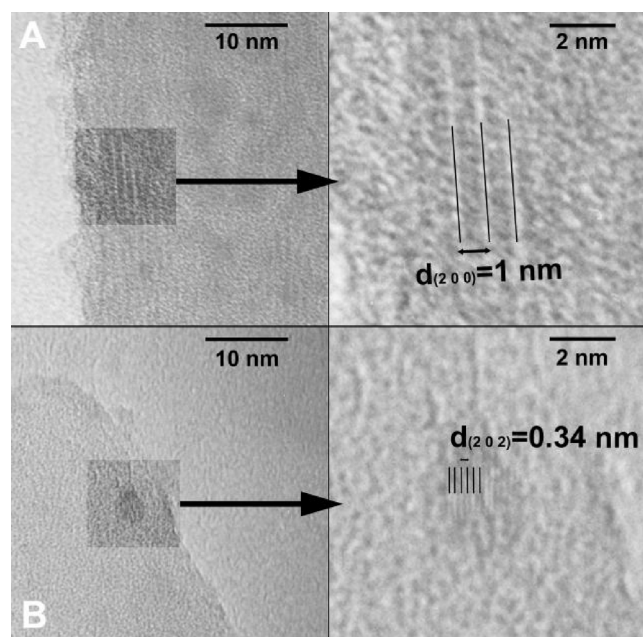
Fig. 4. Representative HRTEM images of the samples studied. The images in this figure were recorded for the sample TECHNOSA-S4. The SEM–EDS analysis performed at magnification 250 provided the chemical composition of the samples studied. This is illustrated in Table 2.

(pore width: 1.6–4.0 nm) while the larger ones by wider slit-like pores.

The acid treatment does not change considerably the fibrous morphology. However, it attacks the ends of the fibers decreasing their length and thick. The attack of the fiber ends increases with the concentration of the acid solution. See for example, the TEM image of the sample TECHNOSA–S6, at magnification 300000. Inspecting the image of the sample TECHNOSA–S2 taken at even higher magnification we discern several "planes" at certain regions of the fiber (see the left – down range of the image). In order to further investigate the structure of the fibers we have examined the samples by HRTEM. This investigation showed that there are fibers with high crystallinity. A representative image is illustrated in Fig. 4A. One may see the crystal planes (2 0 0) which are separated by a distance of about 1 nm, in good agreement to the X-ray and mainly to the electron diffraction results (see Section 3.2). Moreover, this investigation showed that in some cases the fibers are mainly amorphous and the crystals are limited to certain regions of them. A typical image is illustrated in Fig. 4B. We are seeing the crystal planes (2 2 0) separated by a distance of about 0.34 nm.

Inspection of Table 2 shows that the treatment of the natural mordenite (TECHNOSA) with various concentrations of sulfuric acid solutions results in the removal of several cations from the solid. The most vulnerable of the cations seems to be sodium, the amount of which is significantly reduced, even after the mild treatment, and reaches zero in the next three samples. The rest cations are more resistant, with potassium remaining even after treatment with 6 M H_2SO_4. It is very likely that some of these cations are located, in the form of oxides/bases, both in the framework micropores of natural mordenite (Fig. 2) and in the

larger inter-crystal/inter-fiber pores. The correlation between the removals of the various cations, especially of sodium cations, with changes in the texture of the natural mordenite caused by the acid treatment will help us to investigate the positions of these oxides/bases within the mineral before treatment. The oxygen content of the samples is higher than what we would expect if we considered all the cations to be in the form of oxides. This probably suggests that part of the oxygen is due to the water adsorbed by the solid. The Si/Al ratio increases somewhat with acid treatment due to the removal of aluminum ions. The increase in this ratio is smaller when it is compared to that reported in certain cases of acid treatment of synthetic mordenite which, however, are usually performed at higher temperatures [28–32].

Mapping of the cations (not presented here) obtained by SEM-EDS for the untreated natural mordenite shows a uniform distribution. The only exception concerns the K^+ cations which present a more dense distribution at some small aggregates, with a rather granular morphology, presumably corresponding to an amorphous phase. The removal of the cations due to the acid treatment does not change remarkably their distribution. In the particular case of the K^+ cations the acid treatment renders the distribution more uniform by removing these cations preferably from regions with greater density.

3.2. Crystal structure

The crystal structure of the samples studied was investigated by XRD, TEM and ATR-FTIR. Fig. 5 shows the XRD patterns of the samples. Table 3 lists the XRD data obtained from the literature and our measurements. The XRD patterns indicate that the materials are quite crystalline. The positions of the peaks are not practically affected by the acid treatment. This indicates that this treatment does not disturb considerably the material framework. This is in agreement to the literature [28–32]. Table 3 shows that the 2θ experimental values and the corresponding d values are very close to the mordenite literature ones, indicating that the natural mineral we are studying is indeed mordenite. This is also confirmed by the d values obtained through electron diffraction images (not presented here). The above conclusion is corroborated by the fact that the literature relative intensities of the peaks are similar to the experimental ones. The only exception is the peak at 2θ = 27.86° where its relative intensity is higher than the 40% of the maximum peak reported in the literature. It is likely that the crystals of the natural mordenite studied are preferably developed towards the orientation (1 3 2) corresponding to that angle.

We, moreover, observe that acid treatment generally reduces the intensity of the peaks, which may mean a decrease in crystallinity and/or a reduction in the size of the crystals of mordenite. This has reported several times [28,30,32]. However, it is not observed a strong correlation between the decrease in crystallinity and the intensity of the treatment conditions. The effect is more pronounced in the sample TECHNOSA–S2.

The ATR spectra of the samples studied are illustrated in Fig. 6. According to the literature [28–30] the peaks at 805, 1075 and 1223 cm^{-1} correspond to various types of vibrations of the silicate material and the peak at 1635 cm^{-1} to water bending vibrations located inside the zeolite pores. The peaks at 3639 and 3442 cm^{-1} concern the stretching vibrations of the isolated silanol groups (Si−O−H)

Table 2
Atomic composition of the samples studied.

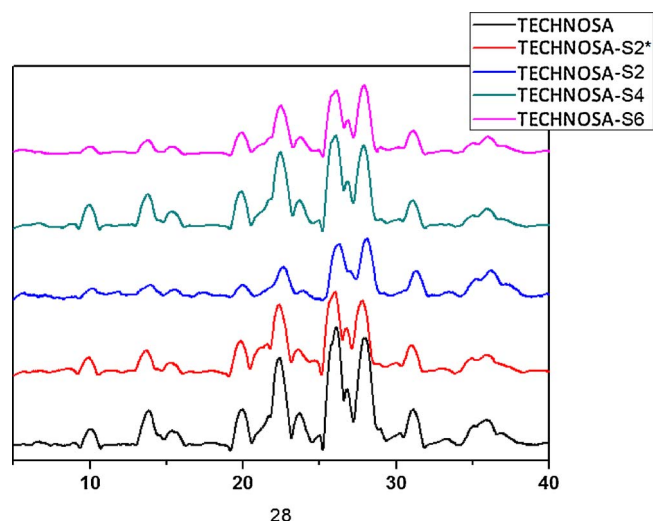| Sample	Si at%	Al at%	Na at%	K at%	Mg at%	Ca at%	Fe at%	O at%	Si/Al at/at
TECHNOSA	20.25	4.41	1.85	0.97	0.49	0.34	0.19	71.50	4.59
TECHNOSA–S2*	19.60	3.60	0.64	0.83	0.43	0.25	0.18	74.47	5.44
TECHNOSA–S2	20.09	3.72	–	0.77	0.41	0.17	0.12	74.72	5.40
TECHNOSA–S4	21.13	3.88	–	0.67	0.41	–	0.16	73.75	5.50
TECHNOSA–S6	20.63	4.07	–	0.64	–	–	–	74.66	5.11

Fig. 5. XRD patterns of the samples studied.

Table 3
Crystallographic data (2θ XRD peak position, relative intensity, Muller indices, Crystal planes distance calculated by XRD and measured by TEM) .

2θ (°)	Relative Intensity	Muller Indices	Distance between the crystal planes [d (Å)]
10.02[a](9.92)[b]	50[a]	2 0 0[a]	8.82[a] (8.91)[b] (9.95–10.5)[c]
13.59 (13.65)	20	1 1 1	6.51 (6.49) −
15.42 (15.37)	10	3 1 0	5.74 (5.76) −
19.94 (19.92)	30	4 0 00	4.45 (4.46) (4.45)
22.78 (22.39)	70	1 5 0	3.90 (3.97) (3.88)
23.97 (23.66)	5	0 0 2	3.71 (3.76) −
25.96 (25.93)	100	2 0 2	3.43 (3.40) (3.4–3.5)
26.67 (26.74)	50	0 6 0	3.34 (3.33) (3.3)
27.86 (27.89)	40	1 3 2	3.20 (3.20) (3.1)
30.53 (30.54)	30	5 3 1	2.93 (2.93) (2.7–2.8)
36.12 (36.02)	10	0 6 2	2.49 (2.49) (2.5)
44.86 (44.92)	15	2 8 2	2.02 (2.02) −
45.47 (46.80)	5	0 6 3	1.99 (1.94) (1.8)
47.05 (48.76)	10	0 10 1	1.93 (1.87) (1.75)
47.81 (−)	3	7 7 0	1.90 − −

[a] literature data (JCPDS # 01-073-1490).
[b] XRD experimental values.
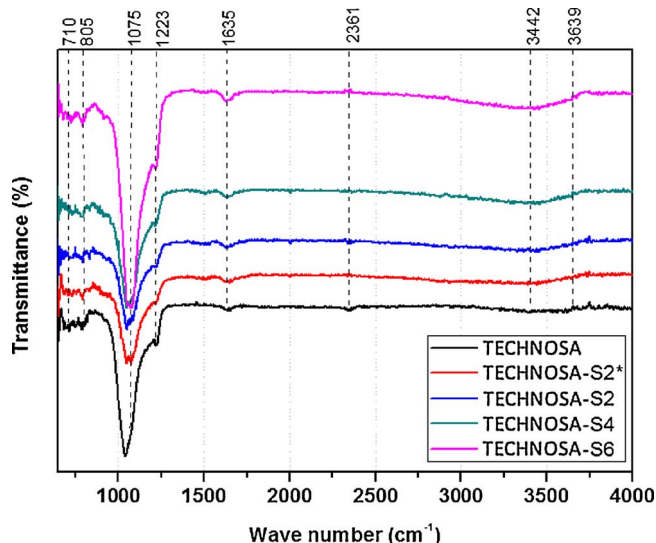[c] TEM experimental values.

Fig. 6. ATR-FTIR spectra recorded for the samples studied.

and water molecules adsorbed on the surface of the material. Finally the peak at 710 cm^{-1} corresponds to the tetrahedral units SiO_4 and AlO_4.

It may be seen that the spectra of the samples studied are quite similar confirming the XRD and TEM findings that the acid treatment does not affect the mordenite framework. However, several minor differences should be discussed. The first concerns the displacement of the main peak at 1075 cm^{-1} to somewhat larger wave numbers after the acid treatment. This indicates that the corresponding vibrations of the natural mordenite framework are sensitive to the removal of the cations from the mordenite pores (Table 2). The second concerns the progressive increase of magnitude of the peak at 1635 cm^{-1} with the concentration of the acid solution. This is most likely associated to the increase of the H_2O/H_3O^+ species located inside the zeolite pores because of the increase of the pore volume in the range of micropores [28,29,31,32] and small mesopores [28–31] (see also below) and the replacement of the cations (mainly Na^+, see Table 2) by H_3O^+. Removal of these cations from the outer surface of the natural mordenite due to acid treatment and their replacement by H_3O^+ is reflected in the increase in the peak size at 3442 cm^{-1}.

In conclusion, the ATR-FTIR spectra corroborate the XRD and TEM findings concerning the stability of the natural mordenite framework. Moreover, these indicate the replacement of the cations (mainly Na^+) by H_3O^+ inside the zeolite pores and in the external surface as well as the increase of the adsorbed water molecules.

3.3. Acidity and ζ-potential

Although the TPD of ammonia is, in effect, the most popular methodology for acidity measurements in zeolites [28–31], in the present contribution we have adopted the joint use of the "equilibrium pH" and "microelectrophoresis" methods because these techniques are more suitable for non-calcined samples working in contact with the liquid phase at relatively low temperatures (below 200 °C) as in our case.

The determination of the equilibrium pH of dense "solid/water" suspension [35–37] is a very simple way for estimating the change in the acidity of the mordenite brought about by the acid treatment. The values of the equilibrium pH are compiled in Table 4.

One may observe that the equilibrium pH is quite high in the untreated sample (TECHNOSA). This can be attributed to the dissolution of basic phases (e.g. sodium oxide) of natural mordenite upon the equilibration of the dense suspension. The acid treatment increases significantly the acidity and this can be attributed to the removal of the aforementioned basic phases and the insertion of H_3O^+ in the mordenite pores. However, a slight decrease in the acidity is observed as the volume and the concentration of the acid solution is increasing. This can be attributed to slight surface dissolution of Al^{3+} ions related to surface acid sites.

A suitable way to approach the surface charge of the samples studied in contact with an electrolytic solution is to measure the microelectrophoretic mobility of the samples and determine ζ-potential, namely the potential at shear plane of the interface developed between the solid surface and the electrolytic solution [38]. ζ-Potential is strongly related to the surface charge. The change in ζ-potential with pH is shown in Fig. 7.

Table 4
Values of the equilibrium pH.

Sample	Equilibrium pH
TECHNOSA	8.11
TECHNOSA–S2*	1.84
TECHNOSA–S2	2.58
TECHNOSA–S4	2.65
TECHNOSA–S6	2.65
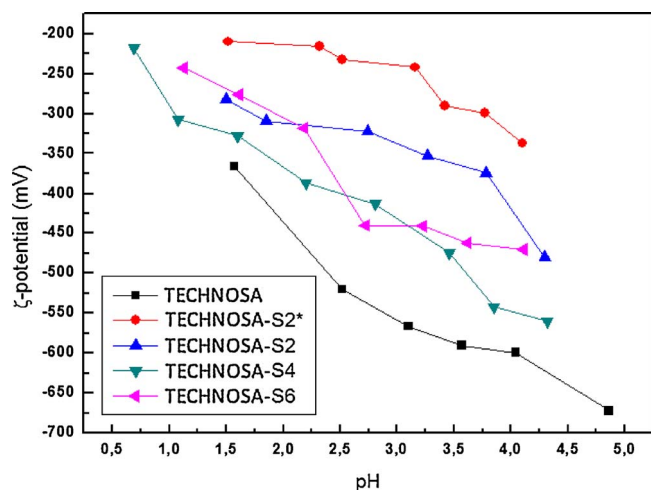
Fig. 7. ζ-potential values determined at various pHs for the samples studied.

Table 5
Textural parameters (Total specific surface area, S_{BET}; Specific surface area outside of micropores, S_{BJH}; Specific pore volume in meso- and macropores, V_{BJH}; Mean pore diameter of meso- and macropores, d_{BJH}) of the samples studied .

Sample	S_{BET} (m^2/g)	S_{BJH} (m^2/g)	V_{BJH} (cm^3/g)	d_{BJH} (nm)
TECHNOSA	16	8.4	0.06	19.5
TECHNOSA–S2*	48	11.7	0.10	31.8
TECHNOSA–S2	231	10.6	0.05	16.5
TECHNOSA–S4	252	12.6	0.06	15.8
TECHNOSA–S6	158	9.1	0.06	24.2

Let's concentrate our attention on the untreated natural mordenite (TECHNOSA). An extremely high negative ζ-potential value was determined at pH = 5. This is because the cations (mainly Na$^+$) are dissolved and removed from the mordenite surface upon the contact of a very small amount of the mineral (10 mg) with a very large amount of electrolytic solution (100 mL). Therefore, the mordenite surface is negatively charged. As pH decreases H$_3$O$^+$ ions are inserted in the mordenite pores and the negative surface charge is partly offset resulting to a decrease of the absolute value of the negative potential. This, however, remains high enough, even at pH = 1. It is very likely that the amount of the H$_3$O$^+$ ions inserted in the very small micropores of the mordenite is not sufficient to compensate entirely the negative surface charge.

The absolute value of the negative potential is smaller in the samples produced through the acid treatment than that determined in the untreated sample. One may imagine that under the strong acidification conditions, a large proportion of the negative charge, resulting from the dissolution of the cations, has already been replaced by H$_3$O$^+$ ions. As with natural mordenite, the reduction in pH brings more H$_3$O$^+$ ions to the mordenite micropores, resulting to a reduction in the absolute value of the negative potential. Because of the uncertainty related to the determination of such high negative potential values, it is not easy relating further the potential curves to the acid treatment conditions.

The low Si/Al ratio (~5) of the natural mordenite and the activated samples is expected to lead to large number of nearest neighbor Al-O(H)-Si sites and thus to high density of quite strong acid sites. This is reflected in the very small values of the equilibrium pH determined for the activated samples (1.84-2.65, Table 4) and mainly in the extremely high negative values of the ζ-potential (in range −700 up to −200 mV, Fig. 7). In fact, these values of the ζ-potential are extremely negative as they compared to those of silica and alumina being for pH < 5 in the ranges 0 to −40 mV and +10 to −10 mV, respectively [39,40]. These, very high negative values determined at low pH (< 5) indicate very high density of negative surface charge and strong tendency of the surface hydroxyls to dissociate releasing protons in the solution. In view of the above one may see that joint measurements of equilibrium pH and ζ-potential provide strong evidences for high density of the quite acidic sites on the surface of the samples studied.

3.4. Texture

The effect of acid treatment to textural features of synthetic mordenite has been reported several times in the past [28–31] but only one time for natural mordenite [34]. The values of the texture parameters of the samples studied are illustrated in Table 5.

It should be noted that the S_{BET} values are determined taking into account the surface of all pores including micropores (up to 2 nm), mesopores (2–50 nm) and macropores (larger than 50 nm) as well as the external surface. On the other hand the parameters determined following the BJH method [41] concern mainly mesopores and to some extent macropores. The most important observation is the very high increase of the BET specific surface area achieved via the acid treatment of the natural mordenite. It increases with the volume and concentration of the sulfuric acid solution up to the sample TECHNOSA–S4 and then it decreases. Taking into account the rather small values of BJH surface area (Table 5, column 3), the increase in the BET surface area can be effortlessly attributed to micropores emptied due to the dissolution of cations located inside them. Comparing the values of sodium content (Table 2, column 4) with the increase in the BET specific surface area (Table 5, column 2) we incline to believe that sodium oxide/base located inside the micropores are mainly dissolved upon the acid treatment bringing about emptying of micropores and thus the impressive increase in the BET specific surface area.

The empting of the micropores can be further investigated by studying the nitrogen adsorption-desorption isotherms of the samples studied. These are illustrated in Fig. 8.

In the small and medium p/p° values the isotherms obtained are of type **I** representative of microporous solids. The abrupt increase in the amount of the adsorbed nitrogen at p/p° values very close to zero due to the acid treatment is indicative of the considerable increase of micropores population mentioned before. It is important to note that this increase is correlated very well to the increase of the BET specific surface area showing once again that this surface is mainly developed inside the framework micropores. However, the small hysteresis loops present at relatively high p/p° values suggest the presence of mesopores and to some extent of macropores, in addition to the predominated micropores. The isotherms in the aforementioned p/p° region belong to H4 type related to the formation of narrow slit-like meso- and macropores. Such a pore shape is in agreement with the fibrous morphology
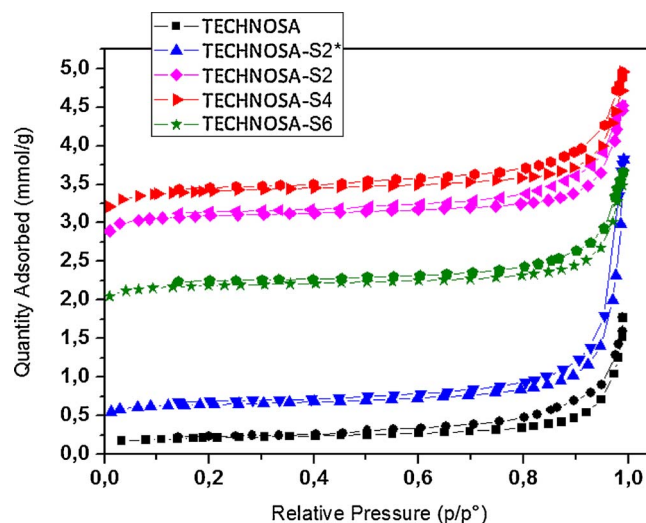

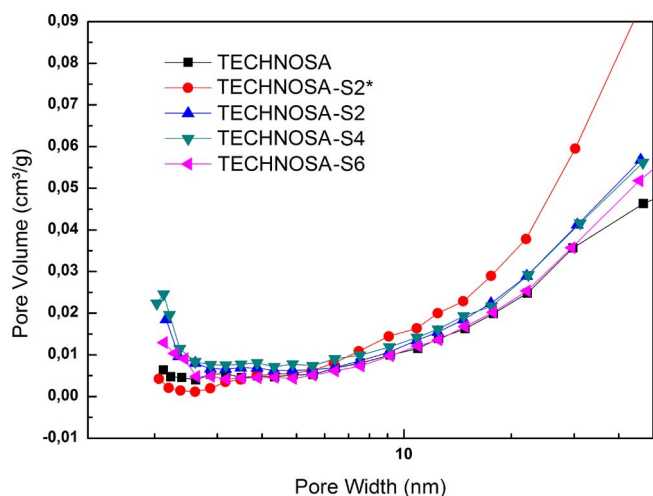Fig. 8. Nitrogen adsorption-desorption isotherms of the samples studied.

Fig. 9. Pore volume distribution of the samples studied in the in the range 2–50 nm.

Fig. 11. Limonene conversion and product distribution over the catalysts studied at 140 °C and reaction time = 2 h under air atmosphere (15 g of liquid limonene, 15 g of tetraethylene glycol dimethyl ether and 1 g of catalyst).

of the samples deduced by electron microscopy images (Fig. 3). The mean pore diameter is varied in the range 15.8–31.8 nm and the pore volume in the range 0.05–0.1 cm^3 g^{-1} (Table 5, columns 5, 4). The mesopores volume distributions are illustrated in Fig. 9.

A rather parabolic distribution is obtained in all cases. The acid treatment with the small volume solution (5 mL, TECHNOSA–S2*) increases considerably the pore volume but at pore sizes greater than 10 nm. This indicates that a significant portion of cations (Table 2) are removed from the relatively large inter-fiber pores upon these mild acid treatment conditions. It seems that under these conditions a portion of the cations removed from the high populated micropores are re-precipitated upon drying inside the less populated mesopores in the range of 2–3 nm leading to a decrease of its pore volume. This is better visualized in Fig. 10.

Inspection of Fig. 10 shows, moreover, that the acid treatment under more severe conditions causes the emptying of small inter-fiber mesopores, mainly those of 2–2.6 nm in addition to micropores. As in the case of micropores the intensity of this effect is maximized in the sample TECHNOSA–S4 and then it decreases. In conclusion, the treatment of the natural mordenite with 2 M and 4 M sulfuric acid solution causes the emptying of the framework micropores and the very small inter-fiber mesopores from sodium oxide/base located inside them resulting to impressive increase in the specific surface area without disturbing seriously its framework.
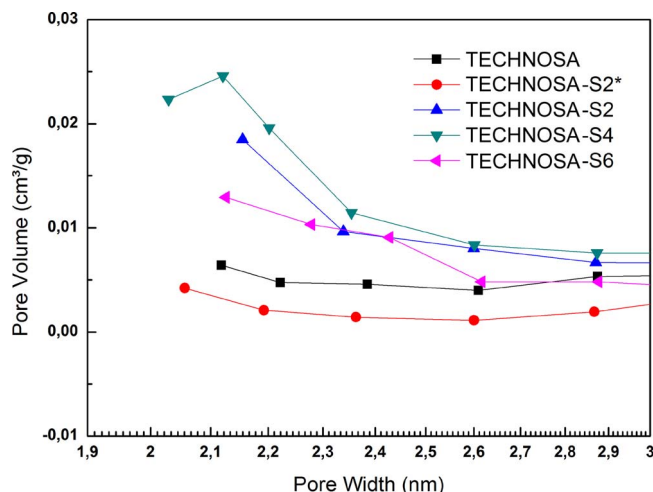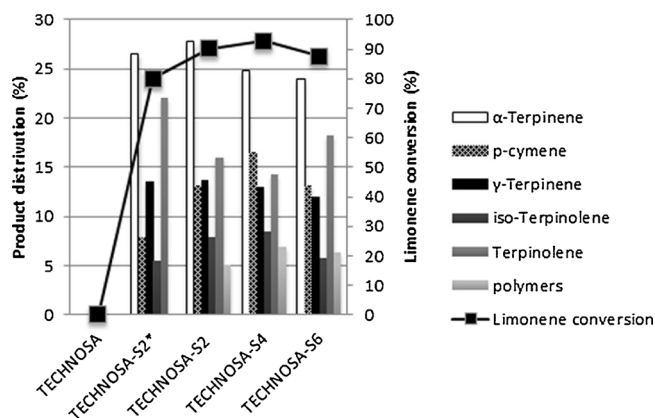

Fig. 10. Pore volume distribution of the samples studied in the in the range 2–3 nm.

3.5. Catalytic activity and reaction mechanism

Experiments were first performed in contact with air in order to evaluate the catalytic activity of the samples studied under oxidative conditions. Representative results at 140 °C are illustrated in Fig. 11.

Preliminary experiments performed without catalyst have shown that limonene is not transformed into p-cymene under our experimental conditions. Moreover, it may be seen that the untreated sample is completely inactive. In contrast, the acid treated samples are proved to be active. Over these samples the reaction mixture consisted of a volatile fraction (α-terpinene, γ-terpinene, p-cymene, terpinolene and isoterpinolene) and a non-volatile fraction (high molecular weight compounds, called "polymers"). A few additional small peaks were present in the chromatograms but their low concentration precluded their identification by GC–MS, so they were neglected.

The absence of 3-menthene, p-menth-1-ene and p-menthane in the reaction mixture precludes disproportionation of limonene or other terpenes under our conditions over the catalysts studied (steps 1 and 3 in Fig. 1). Therefore, the reaction is principally proceeds through the isomerization of limonene followed by dehydrogenation (steps 2 and 5 in Fig. 1). A significant observation is that the conversion of limonene and the relative amount of p-cymene follow the same trend with the BET specific surface area (see Fig. 11 and Table 5). Taking into account that this surface area is principally developed inside the micropores we may conclude that at least one of the steps of the process takes mainly place inside the micropores of the catalysts. It is plausible to assume that limonene isomerization to other terpenes takes place on acid sites located inside the micropores. It involves adsorption of the exocyclic double bond of limonene on these sites forming a primary carbenium ion, followed by displacement of the proton to form the more stable tertiary carbenium ions from which terpinolenes and terpinenes and "polymers" are formed [18,19,11]. As already mentioned, the joint measurements of equilibrium pH and ζ-potential provided clear evidences for high density of quite strong acidic sites on the surface of samples studied. Over the untreated natural mordenite these sites are neutralized by the sodium oxide located in the micropores. The acid treatment dissolves this oxide releasing the acid sites and this is reflected in the drastic decrease of equilibrium pH (Table 4). This easily explains the zero activity observed over the untreated natural mordenite and the considerable activity obtained over the acid activated samples. Thus the critical role of acidity is obvious. The one dimensional main framework channels (12MRc, Fig. 2) with apertures of about 0.67 × 0.7 nm allows the entrance of limonene molecules and the exit of the isomeric products. In contrast, these channels do not accommodate the relatively bulky transition state of the bimolecular disproportionation reaction involving two limonene molecules. This explains the no formation of 3-menthene, p-menth-1-ene and p-
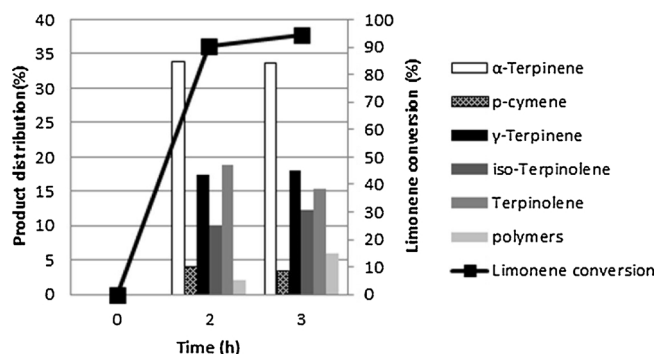
Fig. 12. Limonene conversion and product distribution over TECHNOSA–S2 catalyst at 140 °C under nitrogen atmosphere (15 g of liquid limonene, 15 g of tetraethylene glycol dimethyl ether and 1 g of catalyst).

Fig. 14. Limonene conversion and product distribution over the catalysts studied at 140 °C, reaction time = 2 h and nitrogen atmosphere (15 g of liquid limonene, 15 g of tetraethylene glycol dimethyl ether and 1 g of catalyst).

menthane usually formed over mesoporous solid catalysts [e.g. 11]. The expression of transition state morphoselectivty is obvious in this case.

Inspection of Fig. 11 shows that the sample TECHNOSA-S4 is the most active one concerning both limonene conversion and the product composition in the desired molecule (*p*-cymene). The sample TECH-NOSA–S2 is slightly less active. However, the choice of a catalyst to be developed by the industry in large amounts relies on various parameters among which the cost and mainly the environmental footprint. In this respect is actually important from the environmental burden point of view using more diluted sulfuric acid solutions (2 M instead of 4 M) for catalyst activation. This is the reason for which we are studying further the sample TEHNOSA–S2.

A reasonable question in this point is whether the catalytic action involves dehydrogenation or, alternatively, it is limited to the isomerization and polymerization steps. In order to investigate this point additional catalytic tests were performed under nitrogen atmosphere. Representative results are presented in Fig. 12.

It may be seen that limonene was almost totally transformed to its isomerization products, while aromatization and polymerization were very slightly occurred when these compared to the corresponding tests performed under air (compare the results obtained over TECHNOSA–S2 for reaction time 2 h in Figs. 11 and 12). This is a first indication that atmospheric oxygen promotes both aromatization and polymerization. When the catalytic conversion of limonene was almost complete at about 3 h, the mixture was vacuum-filtrated to remove the catalyst. The catalyst-free mixture was then tested for the aromatization of the isomerization products of limonene. The results are presented in Fig. 13.

It is obvious that the terpenes produced through the catalytic isomerization of limonene are transformed into *p*-cymene under free catalyst conditions while the aromatization of limonene itself, if any, is very slow. Another observation is that the percentage distribution of 'polymers' is increasing under catalyst free-conditions indicating that
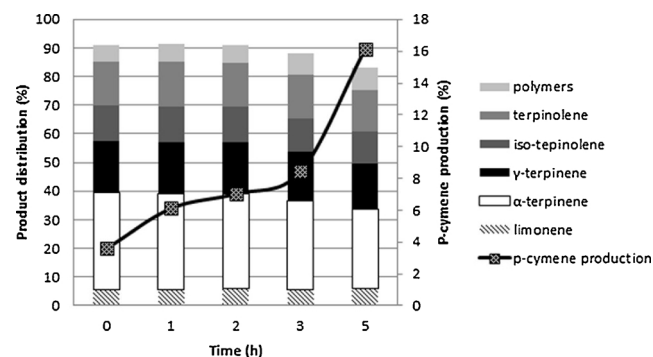
polymerization takes place partly on the catalyst acid sites and partly under free catalyst conditions. Inspection of Fig. 13 shows that aromatization is markedly faster than polymerization at 145 °C under catalyst free conditions.

Taking into account that the catalytic action is mainly limited to isomerization reactions one may expect similar trends for the% conversion of limonene performed in contact with air and nitrogen. This is indeed the case (compare Fig. 11 with Fig. 14). In both cases the activity correlates quite well the specific surface area, maximized over the sample TECHNOSA–S4. In both cases α-terpinene is the major isomerization product. However, the% product distribution over a given catalyst is rather different under air and nitrogen exposure. This is because the dehydrogenation reactivity is not the same for all terpenes produced in the first catalytic step. There is no doubt that% product distributions obtained under nitrogen atmosphere represent more closely the isomerization activity of the samples studied.

As follows from the above, the whole network concerning the conversion of limonene into *p*-cymene involves catalytic isomerization and "polymerization" followed by non-catalytic dehydrogenation and "polymerization" of the produced terpenes. Focusing on the second step it seems plausible assuming that the production of *p*-cymene is initiated by the oxidation of limonene isomerization products in line with previous findings commented in the Introduction [21,22]. Although the second non-catalytic step of the proposed mechanism does not rely on experiments performed in the present contribution, it seems to be in line with the general principles of the physical organic chemistry and recent findings [21,22]. This provides a solid ground for further research concerning its details. Taking into account the above we consider that the initiation of a radical chain reaction is the very first bottleneck of this oxidation pathway. It is due to the high energy required to break a C−H bond, where in our study it is caused by exposing the system to heat, reaction (1).

Initiation: $RH \rightarrow R\cdot + H\cdot$ (1)

Propagation: $R\cdot + O_2 \rightarrow [ROO\cdot] \rightarrow R' + HOO\cdot$ (2)

$HOO\cdot + RH \rightarrow R\cdot + H_2O_2$ (3)

Termination: $HOO\cdot + HOO\cdot \rightarrow O_2 + H_2O_2$ (4)

$HOO\cdot + H\cdot \rightarrow H_2O_2$ (5)

$2H_2O_2 \rightarrow O_2 + 2H_2O$ (6)

Once free radicals are formed, they react with O_2 in a chain process, reaction (2). A peroxy radical ($ROO\cdot$) is formed, where rapid elimination of $HOO\cdot$ accounts the absence of oxygenated organics under these reaction conditions. Then the hydroperoxyl radical $HOO\cdot$ can abstract allylic hydrogen from another terpinene or terpinolene molecule and continue the reaction, reaction (3). Easier H atom abstractions are found in the allylic positions, adjacent to the internal double bond. The

Fig. 13. Catalyst-free aromatization to *p*-cymene of limonene isomerization products: Liquid obtained after limonene isomerization under conditions given in Fig. 12 caption; Air bubbling; Reaction temperature 145 °C.
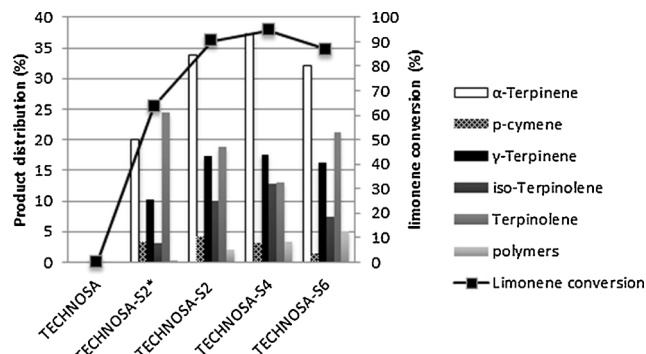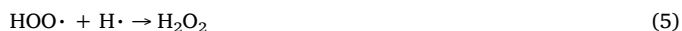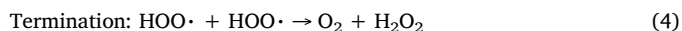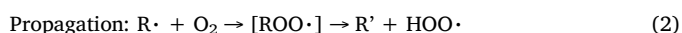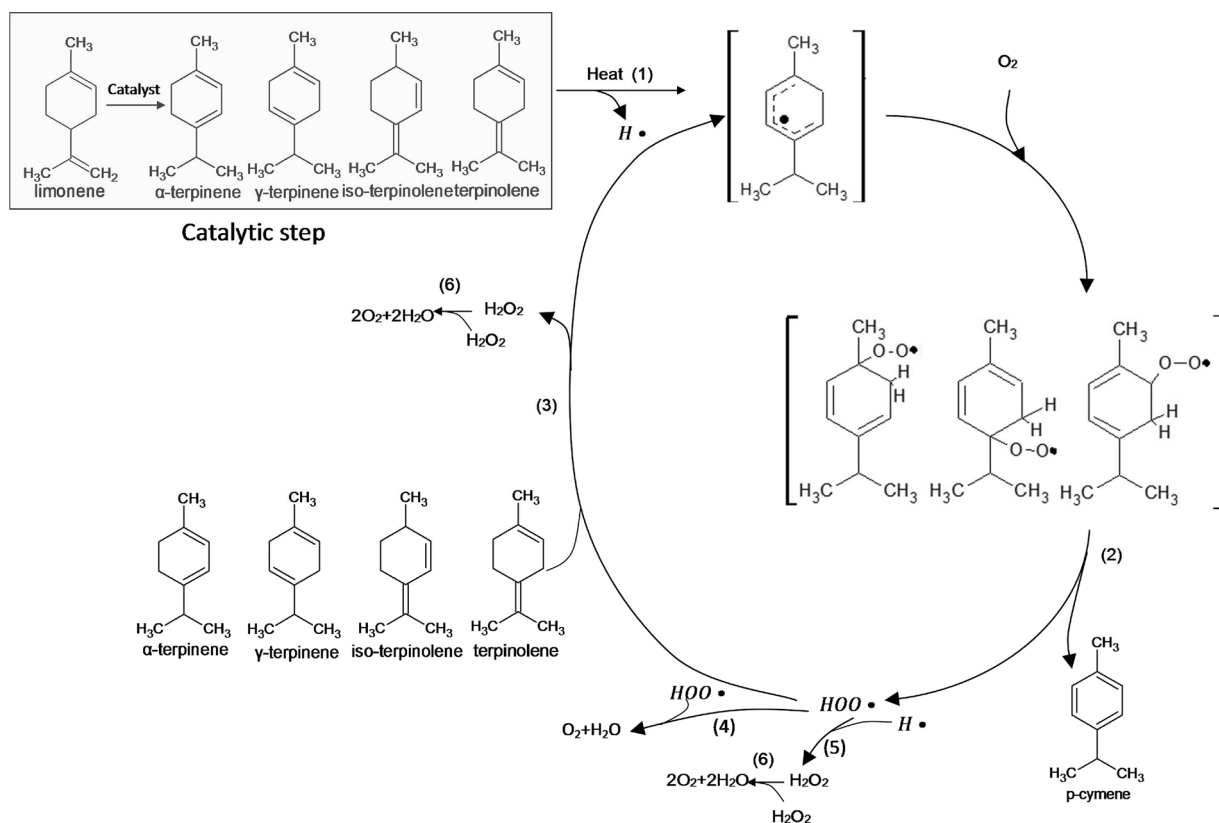
Fig. 15. Mechanistic proposal for the two-step transformation of limonene to *p*-cymene.

allylic radicals, produced by such hydrogen atom abstractions, are stabilized by conjugation of the π orbitals on the allylic C atom and the C atoms of the C=C bond. This means that the unpaired electron becomes delocalized in a π system which involves three C atoms. The more delocalized the electron, the more stable the radical, and as a consequence allylic radicals are more easily formed than alkylic and vinylic radicals [42]. At chain-terminating steps, hydroperoxyl radical can disproportionate to form hydrogen peroxide and oxygen, reaction (4), or they react with hydrogen radicals to form hydrogen peroxide, reaction (5). Hydrogen peroxide can then decompose to water and oxygen, reaction (6) [22]. High molecular weight compounds may be formed as radicals are combined to alkyl and peroxyl dimmers that may be polymerized or decomposed further to non-radical products [42].

In view of the above considerations we propose the mechanistic scheme illustrated in Fig. 15 in order to describe the two steps transformation of limonene to *p*-cymene.

3.6. Optimizing reaction conditions (time and temperature)

The present section deals with the optimization of the limonene into *p*-cymene transformation procedure concerning its reaction temperature and reaction time.

Inspection of Fig. 16 shows that limonene conversion and the yield of *p*-cymene are increasing with the reaction temperature. However, above 140 °C the yield of polymers is increasing much faster compared to that of *p*-cymene. Working at 140 °C is a good compromise ensuring an acceptable *p*-cymene/polymer ratio. Above this temperature the amount of the produced polymer is very high. The aforementioned ratio achieved at 140 °C is very much improved by increasing the reaction time as we may see by inspecting Fig. 17. The% composition of the reaction mixture in *p*-cymene and polymers is equal to 63 and 7.5, respectively after a reaction period of 7 h. Further reaction times do not lead to significant alterations in *p*-cymene content. Thus, working at 140 °C, with a limonene to catalyst ratio equal to 15 and reaction time
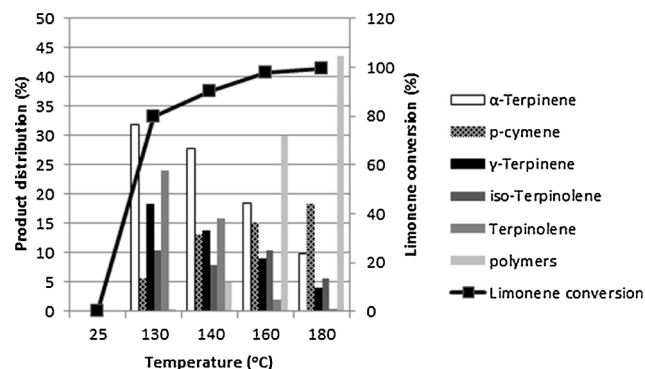

Fig. 16. Limonene conversion and product distribution over TECHNOSA–S2 under air atmosphere at various temperatures and reaction time = 2 h (15 g of liquid limonene, 15 g of tetraethylene glycol dimethyl ether and 1 g of catalyst).

equal to 7 h, a quite high yield of *p*-cymene can be obtained over the THECHNOSA-S2 catalyst, utilizing atmospheric oxygen as a green oxidant.

Using the conversion results presented in Fig. 16 and assuming first order kinetics we calculated the reaction constant (*k*) values at various reaction temperatures ($k = -\frac{\ln(1-X_{limonene})}{t}$, where $X_{limonene}$ and t stand for limonene conversion and reaction time, respectively). Introducing these values in an Arrhenius plot we obtained a very good linear correlation (See Fig. S3), which confirms the aforementioned first order assumption. Using the slope of the straight line obtained we calculated an activation energy value, Ea = 38.8 ± 2.3 kJ mol^{-1}. This relatively low value reflects the high activity exhibited by the acid activated mordenite catalysts.
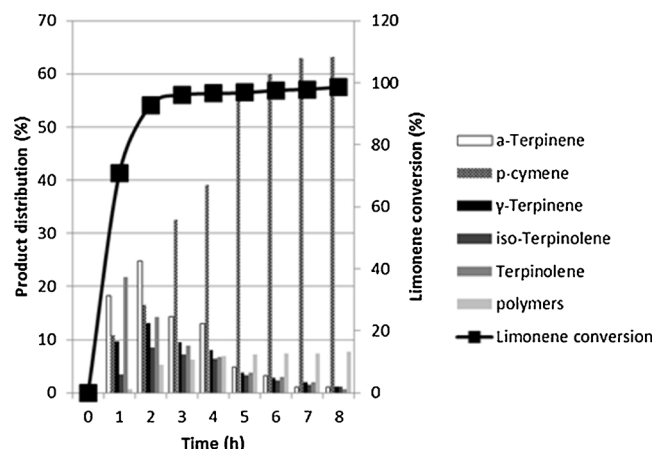
Fig. 17. Limonene conversion and product distribution over TECHNOSA–S2 at 140 °C and various reaction times under air atmosphere (15 g of liquid limonene, 15 g of tetraethylene glycol dimethyl ether and 1 g of catalyst).

4. Conclusions

The activation of natural mordenite with sulfuric acid aqueous solutions of different volumes and concentrations is causing the removal of cations, mainly those of sodium, located inside the framework channels with apertures smaller 1 nm and in the inter-fiber small mesopores of about 2 nm. This brings about a drastic increase of the BET specific surface area (from $16\,\mathrm{m^2 g^{-1}}$ in the untreated mordenite to $252\,\mathrm{m^2 g^{-1}}$ in the TECHNOSA-S4 catalyst) whereas it unmasks negatives surface acid sites. These are transformed into surface acid sites by adsorbing H^+/H_3O^+ ions. The relatively slight increase of the ratio Si/Al due to the removal of Al^{3+} ions leaves rather intact the natural mordenite framework and its fibrous morphology but it decreases somewhat its crystallinity.

The emptying of micropores and small mesopores and the developing of surface acid sites renders the catalytically inactive natural mordenite very active in the catalytic transformation of limonene into *p*-cymene. The increase in the conversion and the percentage composition of *p*-cymene in the reaction mixture follows the increase in the BET specific surface area.

A two-step mechanism is proposed for the aforementioned process: a catalytic step followed by a non catalytic one. This is confirmed by suitably designed experiments.

The first step involves adsorption of limonene via its exocyclic double bond on the acid sites of the catalyst, mainly located inside the micropores, to form the more stable tertiary carbenium ion from which terpinolenes, terpinenes and "polymers" are formed.

The "transition state shape selectivity" manifested by the catalysts studied does not allow the formation of intermediate disproportionation products.

In the second step, non-catalytic oxidation of terpinolenes and terpinenes was found to occur. This was assumed to proceed by abstraction of an allylic hydrogen resulting to free radical (R·) followed by combination with O_2 and radical chain propagation to yield allylic peroxides ([ROO·]), which by elimination of (HOO·) lead to the production of *p*-cymene.

Polymeric compounds are formed as radicals are combined towards alkyl and peroxyl dimmers that may be further polymerized.

Working at 140 °C, limonene to catalyst ratio equal to 15 and reaction time equal to 7 h, a quite high yield in *p*-cymene is obtained over the THECHNOSA-S2 catalyst.

Acknowledgments

We acknowledge the contribution of Dr. A. Seferlis for SEM–EDX analysis and Dr. M. Kollia for TEM analysis of the catalysts at the laboratory of Electron Microscopy and Microanalysis of the University of Patras.

Appendix A. Supplementary data

Supplementary data associated with this article can be found, in the online version, at https://doi.org/10.1016/j.apcatb.2017.11.006.

References

[1] J. Du, H. Xu, J. Shen, J. Huang, W. Shen, D. Zhao, Appl. Catal. A 296 (2005) 186–193.
[2] M.M. Derfer, Kirk-Othmer encycl, Chem. Technol. 22 Wiley-Interscience, New York, 1983, pp. 709–762.
[3] A. Corma, S. Iborra, A. Velty, Chem. Rev. 107 (2007) 2411–2502.
[4] M.A. Martin-Luengo, M. Yates, M.J. Martinez Domingo, B. Casal, M. Iglesias, M. Esteban, E. Ruiz-Hitzky, Appl. Catal. B 81 (2008) 218–224.
[5] M. Eggersdorfer, Ullmann's encyclopedia of industrial chemistry, Terpenes vol 36, Wiley-VCH, Weinheim, 2012, pp. 29–45.
[6] H. Fiege, Ullmann's encyclopedia of industrial chemistry, Cresols and Xylenols vol 10, Wiley-VCH, Weinheim, 2012, pp. 419–460.
[7] D. Buhl, P.A. Weyrich, W.F. Hölderich, Stud. Surf. Sci. Catal. 121 (1999) 191–196.
[8] M. Stratakis, M. Stavroulakis, Tetrahedron Lett. 42 (2001) 6409–6411.
[9] R.J. Grau, P.D. Zgolicz, C. Gutierrez, H.A. Taher, J. Mol. Catal. A 148 (1999) 203–214.
[10] D. Buhl, D.M. Roberge, W.F. Holderich, Appl. Catal. A 188 (1999) 287–299.
[11] M. Kamitsou, G.D. Panagiotou, K.S. Triantafyllidis, K. Bourikas, A. Lycourghiotis, Ch. Kordulis, Appl. Catal. A 474 (2014) 224–229.
[12] M.A. Martin-Luengo, M. Yates, E.S. Rojo, D.H. Arribas, D. Aguilar, E.R. Hitzky, Appl. Catal. A 387 (2010) 141–146.
[13] B.A. Leita, A.C. Warden, N. Burke, M.S. O'Shea, D. Trimm, Green Chem. 12 (2010) 70–76.
[14] M.A. Martin-Luengo, M. Yates, M. Diaz, E.S. Rojo, L.G. Gil, Appl. Catal. B 106 (2011) 488–493.
[15] C. Belver, P. Aranda, M.A. Martin-Luengo, E. Ruiz-Hitzky, Micropor. Mesopor. Mater. 147 (2012) 157–166.
[16] M. Frenkel, L. Heller-Kallai, Org. Geochem. 1 (1977) 3–5.
[17] G.L.K. Hunter, W.B. Brogden Jr., J. Org. Chem. 28 (1963) 1679–1682.
[18] C. Catrinescu, C. Fernandes, P. Castilho, C. Breen, Appl. Catal. A 311 (2006) 172–184.
[19] C. Fernandes, C. Catrinescu, P. Castilho, P.A. Russo, M.R. Carrott, C. Breen, Appl. Catal. A 318 (2007) 108–120.
[20] C. Turek, F.C. Stintzing, Compr. Rev. Food Sci. Food Saf. 12 (2013) 40–53.
[21] J. Rudback, M.A. Bergstrom, A. Borje, U. Nilsson, A.-T. Karlberg, Chem. Res. Toxic. 25 (2012) 713–721.
[22] M. Asikainen, O. Jauhiainen, O. Aaltonen, A. Harlin, Green Chem. 15 (2013) 3230–3235.
[23] W.M. Meier, Zeitschrift für Kristallogr. 115 (1961) 439–450.
[24] M. Tromp, J.A. van Bokhoven, M.T. Garriga Oostenbrink, J.H. Bitter, K.P. de Jong, D.C. Koningsberger, J. Catal. 190 (2000) 209–214.
[25] G.R. Meima, Cattech 3 (1998) 5–12.
[26] S. van Donk, J.H. Bitter, K.P. de Jong, Appl. Catal. A 212 (2001) 97–116.
[27] M. Guisnet, V. Fouche, M. Belloum, J.P. Bournonville, C. Travers, Appl. Catal. 71 (1991) 283–293.
[28] S.K. Saxena, N. Viswanadham, Appl. Surf. Sci. 392 (2017) 384–390.
[29] S.K. Saxena, N. Viswanadham, A.H. Al-Muhtaseb, J. Porous Mater. 23 (2016) 1671–1678.
[30] S. Narayanan, J.J. Vijaya, S. Sivasanker, M. Alam, P. Tamizhdurai, L.J. Kennedy, Polyhedron 89 (2015) 289–296.
[31] K.-H. Chung, Micropor. Mesopor. Mater. 111 (2008) 544–550.
[32] N. Viswanadham, M. Kumar, Micropor. Mesopor. Mater. 92 (2006) 31–37.
[33] M. Boveri, C. Marquez-Alvarez, M.A. Laborde, E. Sastre, Catal. Today 114 (2006) 217–225.
[34] A. Ates, Ch. Hardacre, J. Colloid Interf. Sci. 372 (2012) 130–140.
[35] J. Vakros, C. Kordulis, A. Lycourghiotis, Chem. Commun. (2002) 1980–1981.
[36] K. Bourikas, J. Vakros, C. Kordulis, A. Lycourghiotis, J. Phys. Chem. B 107 (2003) 9441–9451.
[37] K. Bourikas, C. Kordulis, A. Lycourghiotis, Envir. Sci. Techn. 39 (2005) 4100–4108.
[38] G.D. Panagiotou, T. Petsi, K. Bourikas, C.S. Garoufalis, A. Tsevis, N. Spanos, C. Kordulis, A. Lycourghiotis, Adv. Colloid Interf. Sci. 142 (2008) 20–42.
[39] P. Leroy, N. Devau, A. Revil, M. Bizi, J. Colloid Interface Sci. 410 (2013) 81–93.
[40] M. Kawashita, A. Kamitani, T. Miyazaki, N. Matsui, Z. Li, H. Kanetaka, M. Hashimoto, Mater. Sci. Eng. C 32 (2012) 2617–2622.
[41] E.P. Barret, L.G. Joyner, P.P. Halenda, J. Am. Chem. Soc. 73 (1951) 373–380.
[42] C. Backtorp, J.R.T. Johnson Wass, I. Panas, M. Skold, A. Borje, G. Nyman, J. Phys. Chem. A 110 (2006) 12204–12212.